

Theoretical investigation of light scattering characteristics of plate crystals as applied to bistatic polarization laser sensing

O.V. Shefer

*Tomsk State University
Institute of Atmospheric Optics,
Siberian Branch of the Russian Academy of Sciences, Tomsk*

Received March 15, 1999

This paper presents a theoretical investigation of the interaction between optical radiation and a plate crystal as applied to bistatic polarization laser sensing of crystal clouds. A substantiation of the scatterer model choice in the form of an oriented round plate is presented. The relations for polarization characteristics and scattering cross sections as functions of particle size, orientation, and refractive index at arbitrary scattering angles are investigated numerically. A possibility of estimating microphysical, optical, and orientation properties of crystal aerosol from the data of bistatic polarization laser sensing is shown.

Introduction

Crystal clouds can be observed almost everywhere over the Earth surface. Their composition is represented by the variety of shapes and size of particles. One of the most complete classifications of the crystal shapes includes 80 habits.¹ According to the crystallographic growth conditions (i.e., at certain values of the saturating water vapor pressure over ice, temperature, electric field, etc.) one or another type of particles prevails in the cloud.^{2,3} Then, in the temperature range near -20°C and at small water content (as a rule, less than 0.05 g/m^3), clouds principally consist of particles of a plate shape. For example, as it was noted in Ref. 4, crystal clouds over mountains contain about 80% of ice plates. Elongated particles, such as hexagonal columns, needles, plates are observed in practically all mixed clouds.

The character of particle motion in calm atmosphere is caused by their aerodynamic properties and gravitation force. Obviously, crystals are oriented by their maximum cross section along the direction of motion so that the air resistance is maximum. Among all particles of elongated shapes the most stable plates take most stable orientation. They are subject to the least oscillations relative to the preferred orientation plane.

The behavior of particles in the atmosphere depends on the type of air masses motion. Re-orientation of each particle is determined by the difference between the vector of its sedimentation velocity and the wind velocity. The large-scale vortices do not cause chaotic orientation of the ensemble of crystals. Such vortices do transfer a macroscopic volume of a cloud. Small-scale vortices can not change, as a rule, the character of motion of an ensemble of particles, having a preferred orientation because the velocity of such a flux is less than the velocity of the crystal sedimentation.⁵

All force fields affect the features of the air mass circulation. The deep inhomogeneities of the Earth, breaks of geological structures, magnitospheric

fluctuations, electric field – all these factors affect the formation of the structure of the atmosphere.⁶ As a rule, the presence of a force field favors stable orientation of particles in space. For example, the effect of electric field leads to the strict orientation of elongated particles. However, the effect of the electric field on the ensemble of crystals significantly depends on their shape and initial orientation.^{5,7,8}

Numerous investigations showed that ice clouds mostly consist of the systems of particles of some dominating orientation. The mechanism of light scattering on such crystals significantly differs from that on spheres or randomly oriented particles. The peculiarity of light scattering on non-spherical oriented particles is the pronounced anisotropy of the scattering properties. It is just this effect that causes anomalous optical phenomena observed in the atmosphere.⁹

Lidar methods of sounding are now widely used to study crystal clouds. Analysis of polarization state of a received signal is important for such investigations.¹⁰ This is explained by the fact that the polarization of an incident radiation can vary because of variations in the microphysical, optical, and orientation properties of scatterers.

High potentialities in study of the upper and middle atmosphere can be realized by use of remote sounding with a bistatic polarization scanning lidar. Researchers note some important advantages of this method as compared with the traditional monostatic one.^{11,12} At sounding of crystal clouds by means of such a lidar, one can obtain the maximum possible intensity of return signal along with the specific polarization properties characteristic of the certain type of particles. It should be noted that the theoretical findings used in the monostatic laser sounding are used in interpreting the data of bistatic sounding of crystal clouds.

The process of scattering of polarized radiation on an oriented plate is considered in this paper as applied to the bistatic sounding. The choice of such a model is caused by the following factors.

Ice plates are always present in the crystal and mixed clouds.

Optical phenomena observed in the atmosphere, for example, parheliion, sun and moon pillars, anomalous backscattering are caused by the presence of ensembles of oriented crystals.¹³⁻¹⁵ The model proposed can be used for studying these effects.

Plates, as the most stable particles in air flow, can be used as "tracers" for determining the wind direction and diagnostics of the effect of physical fields.

A high-amplitude signal is recorded by the receiving device at specular reflection from the oriented plate-shaped crystals. As was shown in Ref. 16, particles of other shapes can form the return signal, the intensity of which is more than three orders of magnitude lower than the intensity of the signal reflected from plates. The inverse problem on determining the size of such crystals was solved based on the study of anomalous backscattering at monostatic sounding.¹⁶ One should note that the geometrical parameters of the plates, their number density, and orientation are related to certain physical conditions in the atmosphere which at the same time determine the cloud structure as a whole.^{2,3}

Polarization characteristics of scattered radiation

For remote sensing of atmospheric formations by means of lidars, it is necessary to theoretically study the process of scattering of optical radiation in a disperse medium. Thus the numerical model of a scatterer should relate the principal parameters of a pulse scattered along a direction toward the receiver to the microphysical and optical parameters of a medium sounded.

When selecting the crystal model, it is necessary to take into account the following properties: nonsphericity in a geometrical meaning, preferred orientation and high frequency of occurrence of such crystals in the atmosphere. In this connection the optical model of a polydisperse medium consisting of plate-type crystals, quite adequately corresponds to real formations, in particular, to cirrus clouds.

The optical model of a round plate is presented in Ref. 17 as applied to the bistatic polarization laser sounding of crystal clouds. The relationships for cross sections of light scattering into the backward hemisphere are obtained in approximation of the method of physical optics as some combinations of elements of the scattering phase matrix.

According to the laws of propagation of electromagnetic radiation, one should describe the process of scattering in cirrus clouds in a vector form.⁹ It is especially important when considering the scattering of optical radiation on particles that have a preferred orientation. The regular position of crystals in space leads to the anisotropy of scattering.

It is known that the Stokes parameters provide for a complete description of a polarized radiation. Four

measurement channels can be used at single-frequency laser sounding, according to the number of these parameters. Each of them is proportional to the corresponding cross section, i.e.,

$$\sigma_{\pi_i} = \omega I_{\pi_i}, \quad i = 1, 2, 3, 4, \quad (1)$$

where I_{π_i} are the Stokes parameters of scattered radiation, and σ_{π_i} are the cross sections. The proportionality coefficient ω includes all necessary parameters, which enter the lidar equation, as factors. Obviously, the value ω is the same for all four equations relating the Stokes parameters with the cross sections. Let us note that although it is impossible to determine the values σ_{π_i} from the lidar equations without attracting some *a priori* information, their ratios

$$P_i = \frac{I_{\pi_i}}{I_{\pi_1}} = \frac{\sigma_{\pi_i}}{\sigma_{\pi_1}}, \quad i = 2, 3, 4, \quad (2)$$

can be measured directly in the experiment. At laser sounding of disperse media one often use a transmitter that transforms the linearly polarized radiation, or radiation with circular polarization. So let us consider the values p_2 and p_4 for linear and circular polarization of the incident radiation in analyzing the polarization properties of scattered radiation.

The following relationships¹⁷ are valid for the cross sections σ_{π_i} :

$$\begin{aligned} \sigma_{\pi_1} &= W \left\{ M_{11} + \frac{I_2}{I_1} M_{12} + \frac{I_3}{I_1} M_{13} + \frac{I_4}{I_1} M_{14} \right\}, \\ \sigma_{\pi_2} &= W \left\{ M_{21} + \frac{I_2}{I_1} M_{22} + \frac{I_3}{I_1} M_{23} + \frac{I_4}{I_1} M_{24} \right\}, \\ \sigma_{\pi_3} &= W \left\{ M_{31} + \frac{I_2}{I_1} M_{32} + \frac{I_3}{I_1} M_{33} + \frac{I_4}{I_1} M_{34} \right\}, \\ \sigma_{\pi_4} &= W \left\{ M_{41} + \frac{I_2}{I_1} M_{42} + \frac{I_3}{I_1} M_{43} + \frac{I_4}{I_1} M_{44} \right\}, \\ W &= \frac{k^2}{\pi} \left(\frac{1 + \cos \vartheta}{2} \right)^2 G_0^2(\vartheta, \varphi), \end{aligned} \quad (3)$$

where I_i ($i = 1, 2, 3, 4$) are the Stokes vectors of the incident radiation, $k = 2\pi/\lambda$ is the wave number, λ is the wavelength, $G_0(\vartheta, \varphi)$ is the angular function which is the Fraunhofer integral, ϑ is the scattering angle, φ is the azimuth angle, and M_{ij} are the elements of Mueller matrix. One should note that the elements of this matrix can be represented in the form of the product $M_{ij} = F(a) A_{ij}$ with the error not greater than 2%.¹⁸ The function $F(a)$ primarily depends on the plate size a , while the values A_{ij} depend on the combination of Fresnel coefficients, on the orientation of the polarization plane, and on the angles relating the components of the incident electromagnetic radiation to the corresponding components of the scattered radiation.

It is known that the Mueller matrix bears all principal information on the properties of the scattering

volume, directly related to variations of the incident radiation. All 16 elements of the backscattering phase matrix (BSPM) of the non-spherical particles can differ from zero. Setting all necessary parameters of the incident radiation and the plate, fixing the positions of the source, the scatterer and the receiver, one can determine the scattering matrix elements. The depolarization ratio

$$D = (M_{11} - M_{22}) / (M_{11} + M_{22}). \quad (4)$$

is one of the parameters that characterize the non-sphericity of a scatterer.¹⁹

The scattering phase matrix for spherical or non-spherical but randomly oriented particles has the diagonal form, and only one of its elements bear information, i.e., $M_{11} = M_{22}$, hence, $D = 0$. Let us note that at the specular reflection from a plate only diagonal elements of the backscattering phase matrix differ from zero, and their absolute values are equal to each other.²⁰ However, for the case of bistatic sounding, only two elements of the total 16 elements are equal to zero (as at the arbitrary incidence and scattering of radiation).¹⁷ Obviously, the change of the polarization state of incident radiation is observed in this case after specular reflection from the plate.

Thus, let us numerically study the light scattering characteristics which are interesting for the bistatic laser sounding, namely, the study of normalized values for the cross sections, such as P_2 and P_4 , the study of the absolute value of the cross section σ_{π_i} , and of the depolarization ratio D . Let us use the corresponding formulas (2)–(4).

The optical arrangement of bistatic sounding was presented in Ref. 17, where the absolute coordinate system was introduced, with which the positions of source, receiver, and particle are related by the corresponding pair of angles φ_i, ϑ_i ($i = 1, 2, 3$). Let us note that it is too a cumbersome problem to illustrate the scattering characteristics under study as functions of the input parameters such as φ_i, ϑ_i ($i = 1, 2, 3$). It is conventional to describe the rotation of a body in space relative to a Cartesian coordinate system by Euler matrix. We used such a relationship for the coordinate systems related to the source and the plate.

In the framework of this paper, the orientation of polarization plane of the incident radiation relative to the normal to the incidence plane is determined by the angle γ , and the orientation of the plate relative to the sounding plane is determined by the angle β . The remaining angle α prescribes the angle of rotation of a fixed point on the plate relative to the normal to its base. So let us represent the parameters under study as functions of these angles, keeping in mind that α, β , and γ are determined by a combination of the angles ϑ_1, φ_1 and ϑ_3, φ_3 . Fixing $\vartheta_1, \varphi_1, \varphi_3$ and varying ϑ_3 (or fixing $\vartheta_3, \varphi_1, \varphi_3$ and varying ϑ_1), we observe simultaneously change in β .

The change of γ is determined by variations of φ_1 (or φ_3) at the three other angles fixed. Let us note that the change of the polar angle, for example, ϑ_3 , at the angles ϑ_i and φ_i ($i = 1, 2, 3$) different from zero, implies only insignificant change of γ (in the limits of 5–10°). In its turn, changing only the azimuth angle, for example, φ_3 , we observe insignificant change of β . Calculations of the light scattering characteristics shown in the figures below were carried out for the incidence radiation wavelength of 10.6 μm that corresponds to the wavelength from the atmospheric transmission window. Obviously, the ratios of the cross sections (and depolarization ratio) do not depend on the wavelength, while their absolute values depend. The wave characteristic, namely, the wave number is incorporated into the relationships (3) determining the cross sections σ_{π_i} non-linearly as k^2 . Obviously, the reflected signal of greater amplitude corresponds to a shorter wavelength, other input parameters being fixed.

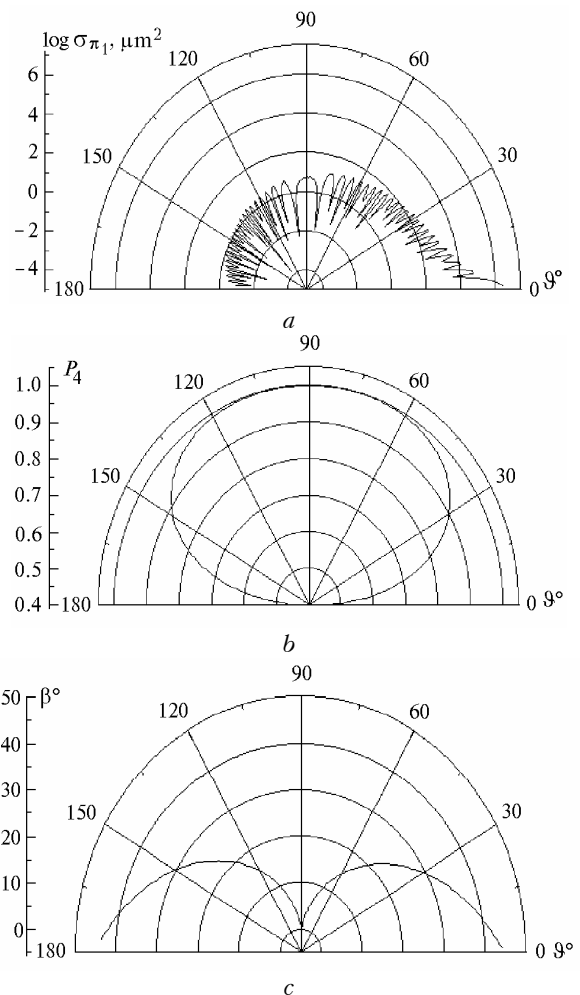


Fig. 1. Angular dependence of the scattering cross section $\sigma_{\pi_1}(\vartheta)$: $a = 125 \mu\text{m}$, $\lambda = 10.6 \mu\text{m}$, $\tilde{n} = 1.31 + i \cdot 10^{-4}$ ($I_4/I_1 = 1$; $I_2 = I_3 = 0$) (a); the dependence $P_4(\vartheta)$ at the same parameters (b), and correspondence of the angles ϑ and β used for calculating σ_{π_1} and P_4 (c).

The dependences $\sigma_{\pi_i}(\vartheta)$ and $P_4(\vartheta)$ for circular polarization are shown in Figs. 1a and b (ϑ is the angle between the directions of receiving and specular reflection). The calculations were made for $\vartheta_1 = 0$, $\vartheta_2 = 91^\circ$, $\varphi_1 = \varphi_2 = \varphi_3 = 0$ and for the change of ϑ_3 from -44 to 44° . The dependence $\sigma_{\pi_i}(\vartheta)$ oscillates as ϑ increases with a quick decrease of the amplitude maximum. Obviously, σ_{π_i} has the maximum value at $\vartheta \rightarrow 0$. When ϑ changes from 0 to 15° , the mean value of the cross section decreases by approximately four orders of magnitude. The value σ_{π_i} at large ϑ , for example, from the range 30 to 90° , decreases by only one order of magnitude. By comparing the values σ_{π_i} at $\vartheta \approx 0$ and 180° , one can see that their difference reaches almost 10 orders of magnitude. According to Figs. 1b and c, the increase of the value $P_4(\vartheta)$ is directly related to the decrease of β . Polarization properties are most pronounced at large β angles, in particular, at $\beta > 20^\circ$. Thus, the information content of the characteristics shown in Figs. 1a and b, is higher at ϑ varying in the range from 0 to 10° and at $\beta > 20^\circ$.

Figure 2 presents the dependences $\sigma_{\pi_1}(\beta)$ at circular polarization of the incident radiation for different ϑ . The increase of oscillations of $\sigma_{\pi_1}(\beta)$ is observed as ϑ increases. The scattering cross sections have practically linear dependence at small ϑ and β angles.

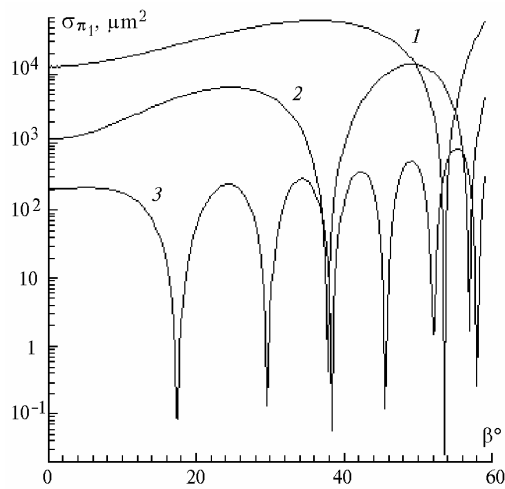


Fig. 2. Dependences of $\sigma_{\pi_1}(\vartheta)$ at different ϑ : $\vartheta = 5^\circ$ (1), 10° (2), 30° (3); $\lambda = 10.6 \mu\text{m}$, $a = 125 \mu\text{m}$, $\tilde{n} = 1.31 + i \cdot 10^{-4}$ ($I_4/I_1 = 1$; $I_2 = I_3 = 0$).

The dependences σ_{π_1} , D , P_2 on the angles ϑ and γ for linear polarization of incident radiation are shown in Fig. 3. The values $\gamma = 90^\circ$ and 270° represent the case when one of the components of the electric vector, for example, \mathbf{E}_1 , is perpendicular to the polarization plane of the incident radiation, and at $\gamma = 0^\circ$ and 180° \mathbf{E}_1 is parallel to it. All three plots have mirror symmetry relative to $\gamma = 180^\circ$. There is no change of the polarization of the incident radiation observed at $\gamma = 0^\circ$ and 180° , i.e., $D = 0$ and $P_2 = 1$. It is seen from Figs. 3b and c that the relative values such as D and P_2 practically do not depend on the angle ϑ .

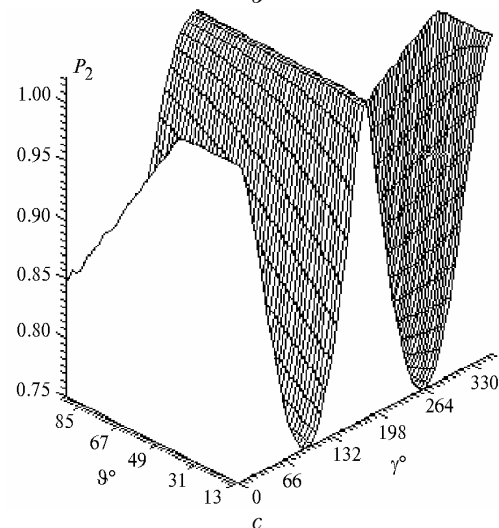
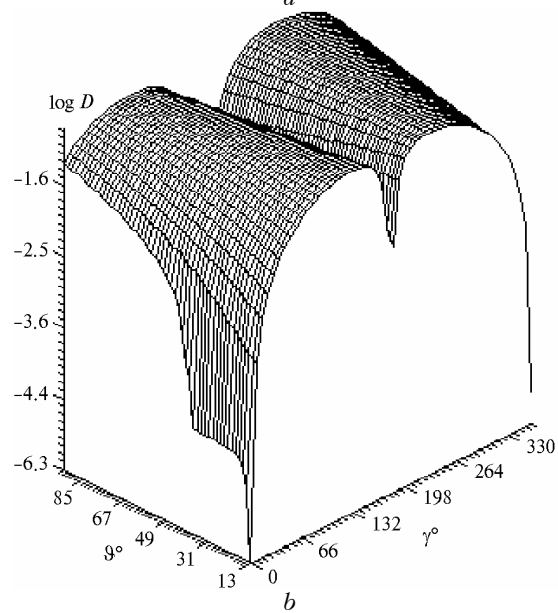
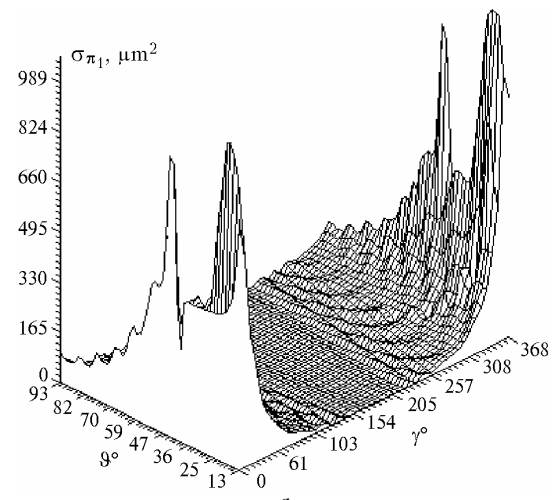


Fig. 3. The function $\sigma_{\pi_1}(\gamma, \vartheta)$ at linear polarization of incident radiation, $a = 125 \mu\text{m}$, $\lambda = 10.6 \mu\text{m}$, $\beta = 20^\circ$, $\alpha = 180^\circ$, $\tilde{n} = 1.31 + i \cdot 10^{-4}$ ($I_2/I_1 = 1$; $I_4 = I_3 = 0$) (a); depolarization ratio D at the same parameters (b) and the dependence of P_2 at the same parameters (c).

The parameters $\sigma_{\pi_1}(\gamma)$, $D(\gamma)$, and $P_2(\gamma)$ are presented in Fig. 4 for linear polarization of incident radiation. The greater is β , the less is the backscattering cross section $\sigma_{\pi_1}(\gamma)$ (Fig. 4a). As the angle β increases, the maxima of the depolarization ratio (Fig. 4b) increase, and the minima of P_2 (Fig. 4c) become lower. The variation of the curves 1 and 2 with ϑ are practically the same. Let us remind that $\sigma_{\pi_1}(\gamma)$, $D(\gamma)$, $P_2(\gamma)$ marked by the number 1 in Fig. 4 have been already shown in Fig. 3 in a 3D representation, as $\sigma_{\pi_1}(\vartheta, \gamma)$, $D(\vartheta, \gamma)$, $P_2(\vartheta, \gamma)$.

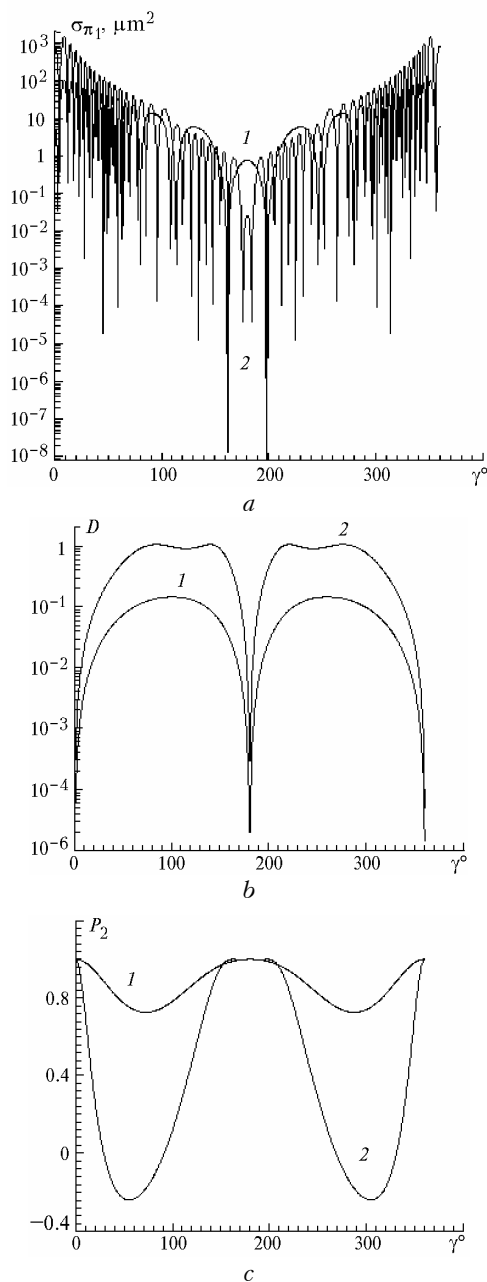


Fig. 4. Dependences of σ_{π_1} , D , P_2 on γ at different orientation of the plate: $\beta = 20^\circ$ (1); $\beta = 40^\circ$ (2); $a = 125 \mu\text{m}$, $\tilde{n} = 1.31 + i \cdot 10^{-4}$, $\lambda = 10.6 \mu\text{m}$ ($I_2/I_1 = 1$; $I_4 = I_3 = 0$).

Figure 5 shows the dependence $P_2(\gamma)$ at linear polarization of incident radiation for different refractive indices n and different orientation of the plate β . Let us note that the greater is the angle β , the greater is the difference between the polarization characteristic $P_2(\gamma)$ at the same changes of the optical properties of the particle. The calculated dependences of the dimensionless parameter $P_2(\gamma)$ at $\beta = 20^\circ$ and imaginary part of the complex refractive index $\chi = 10^{-4}$ for the real parts of the refractive index $n = 1.42$ and 1.20 (are marked in Fig. 5 by the numbers 1 and 2, respectively) differ from each other by no more than 0.15. The minimum values of the cross section ratio $P_2(\gamma)$ for the same refractive indices (number 3 in Fig. 5 corresponds to $n = 1.42$, and 4 is for $n = 1.20$) differ at large $\beta = 45^\circ$ by approximately 0.4. Then it is obvious that the most informative data in estimating the refractive index are the values P_2 at large β angles. It is seen from Fig. 5 that each curve P_2 at the interval $[0, 180^\circ]$ is not symmetrical. So orientation of the plane of wave incidence can be determined unambiguously. One can change the angle γ in experiment by turning the lidar around its axis. As a result, some curve will correspond to the unknown parameters β and n . Thus, there is a possibility of determining the orientation angle β and the refractive index n using the polarization characteristic P_2 .

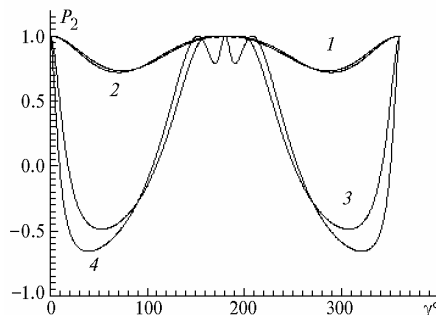


Fig. 5. Dependence of P_2 on γ at different refractive indices: $n = 1.42$ (1) and $n = 1.20$ (2) at $\beta = 20^\circ$; $n = 1.42$ (3) and $n = 1.20$ (4) at $\beta = 45^\circ$; $\alpha = 180^\circ$, $\chi = 10^{-4}$, $a = 125 \mu\text{m}$, $\lambda = 10.6 \mu\text{m}$ ($I_2/I_1 = 1$; $I_4 = I_3 = 0$).

One should note that the light scattering characteristics shown in Figs. 3–5 were considered in the coordinate system chosen so that the plate axis lies in the reference plane (azimuth angle $\varphi = 0$). In this case we observe mirror symmetry of the parameters $\sigma_{\pi_1}(\gamma)$, $D(\gamma)$, $P_2(\gamma)$ relative to $\gamma = 180^\circ$. The input parameters for determining the values $\sigma_{\pi_1}(\gamma)$, $D(\gamma)$, and $P_2(\gamma)$ shown in Fig. 6 were $\vartheta_1 = 20^\circ$, $\vartheta_2 = 127^\circ$, $\vartheta_3 = 30^\circ$, $\varphi_1 = 10^\circ$, $\varphi_2 = 4^\circ$, φ_3 changed from 0 to 360° . The calculations were carried out for the case when all Euler angles α , β , and γ (Fig. 6d) and azimuth angle φ are different from zero. In this case mirror symmetry of the dependences $\sigma_{\pi_1}(\gamma)$, $D(\gamma)$, $P_2(\gamma)$ is broken, and the extrema are displaced. This peculiarity can be used for determining the particle position in space relative to the reference plane.

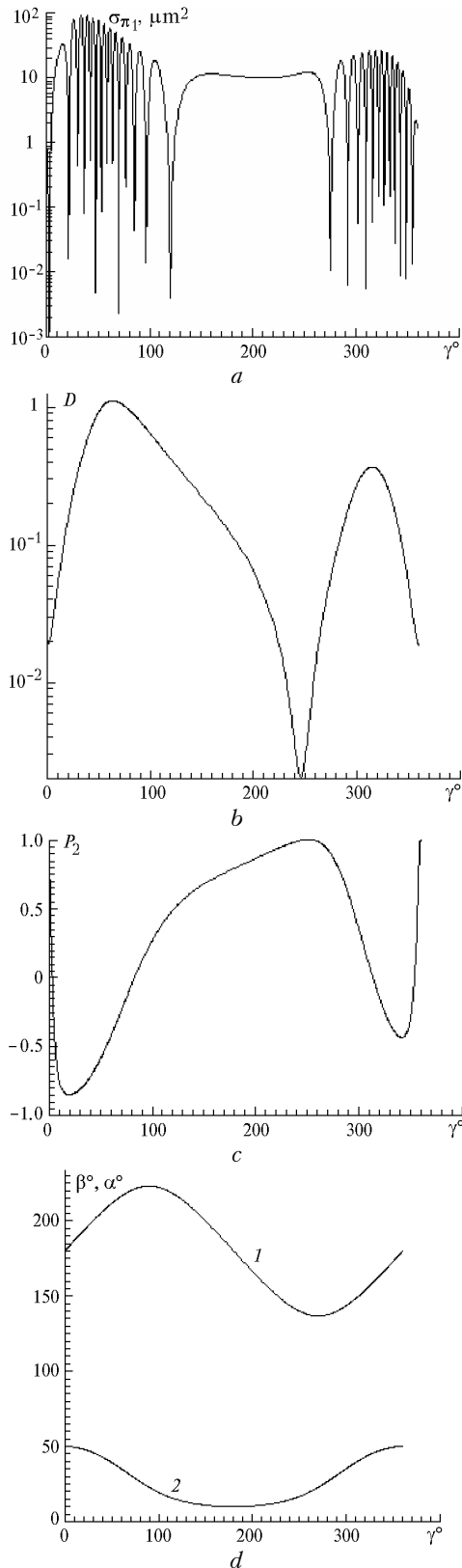


Fig. 6. Dependences $\sigma_{\pi_1}(\gamma)$, $D(\gamma)$, $P_2(\gamma)$, $a = 125 \mu\text{m}$, $\tilde{n} = 1.31 + i \cdot 10^{-4}$, $\lambda = 10.6 \mu\text{m}$ ($I_2/I_1 = 1$; $I_4 = I_3 = 0$) (a), (b), (c); correspondence of the angles α , β , and γ used for calculating the dependences shown in Fig. 6: curve 1 is $\alpha(\gamma)$, curve 2 is $\beta(\gamma)$ (d).

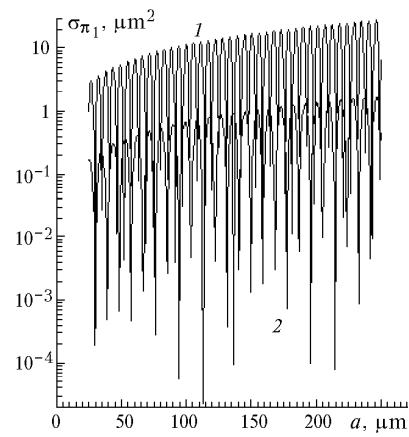


Fig. 7. Dependence of σ_{π_1} on the plate radius a at different orientations: $\beta = 10^\circ$ (1), $\beta = 40^\circ$ (2), $\tilde{n} = 1.31 + i \cdot 10^{-4}$, $\lambda = 10.6 \mu\text{m}$.

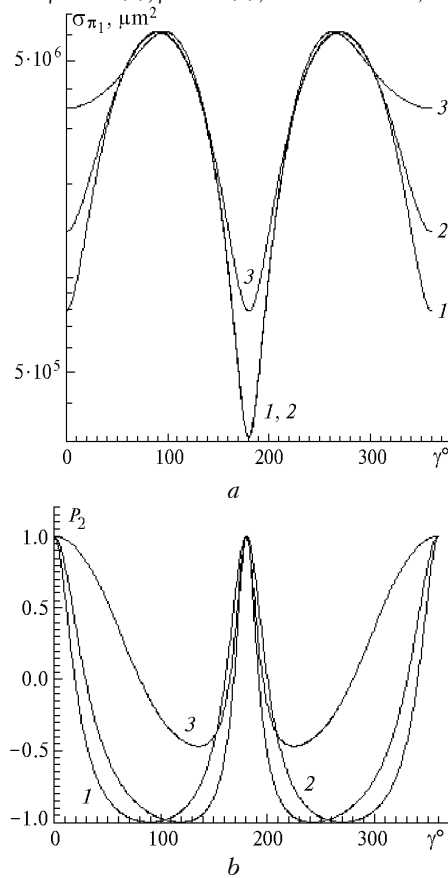


Fig. 8. The dependences $\sigma_{\pi_1}(\gamma)$ and $P_2(\gamma)$ at different sounding directions ϑ_1 : $\vartheta_1 = 0$ (1); 10° (2); 40° (3).

The dependence of σ_{π_1} on the plate radius at its different orientation in space is shown in Fig. 7. The increase of σ_{π_1} is proportional to the increase of the plate size. Such character of the dependence of the backscattering cross section on the disk diameter was observed for the particle model in the case of monostatic sounding.¹⁶ Moreover, we have managed to obtain the interpretation procedures for determining the plate size spectrum and its flatter from the data of monostatic

sounding based on numerical study of the anomalous backscattering coefficient.¹⁶ Let us note that the depolarization ratio and the backscattering cross section ratio do not depend on the particle size.

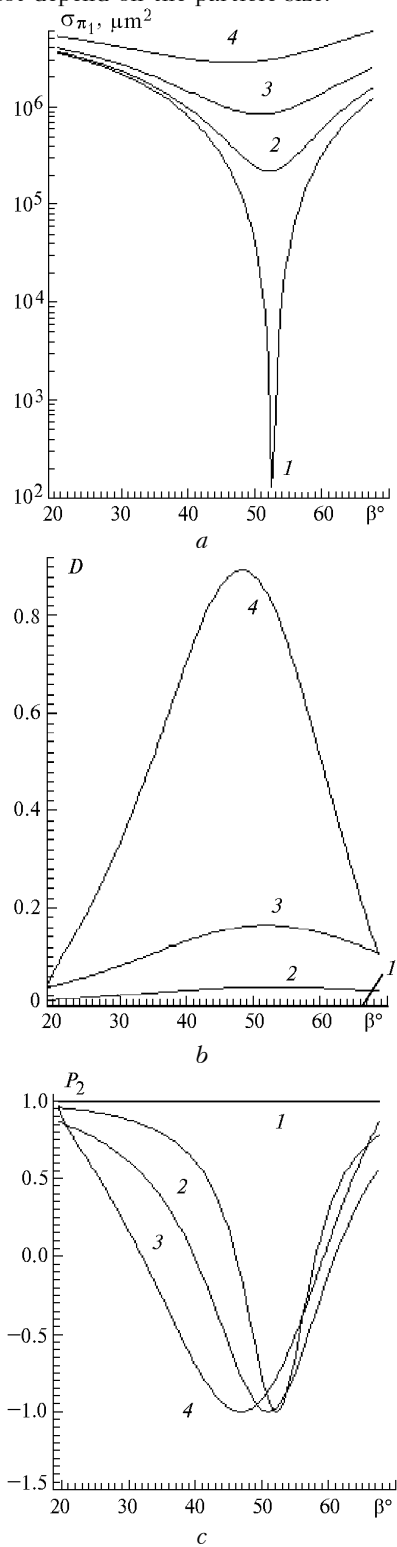


Fig. 9. The dependences $\sigma_{\pi_1}(\beta)$, $D(\beta)$, and $P_2(\beta)$ at different positions of a source and receiver, $\vartheta_1 \in (-79^\circ, 86^\circ)$, $\varphi_1 = 0$, $\vartheta_2 = 100^\circ$, $\varphi_2 = 0$ (1), 10° (2), 20° (3), 40° (4).

Figure 8 illustrates the cross section σ_{π_1} and the cross section ratio, such as $P_2 = \sigma_{\pi_2}/\sigma_{\pi_1}$, in the case of specular reflection ($\vartheta = 0$) at linear polarization of incident radiation as functions of the angle γ for different ϑ_1 . The parameters σ_{π_1} and P_2 in the case of specular reflection take extreme values at the points $\gamma = 90^\circ i$ (i is an integer number). Such dependences we have already observed in Fig. 4 at $\vartheta \neq 0$. The position of maxima and minima depend on β .

Figure 9 shows the dependences of σ_{π_1} , D , and P_2 (for $\vartheta = 0$) on the plate orientation β at linear polarization of the incident radiation. There are minima in the dependences σ_{π_1} , D , and $P_2(\beta)$ and a maximum of $D(\beta)$ at the maximum values γ in the range of $\beta \approx 50^\circ$. The positions of the extrema depend on the values α , β , and γ .

The revealed peculiarities of the relationship between the polarization characteristics and the values \tilde{n} , β , and γ make it possible to construct an interpretation procedure for determining the orientation and refractive index of plates from the data of polarization laser sounding when the source and the receiver coincide.¹⁸ Such dependences of P_2 and P_4 are shown in Figs. 1b, 3c, 4c, 5, 8b, and 9b. The change of polarization characteristics is related not only to the variations of orientation, but also to the crystal shape and size.² It is unlikely that one can obtain reliable data from the polarization characteristics when sounding the clouds of complex structure with a monostatic lidar without attracting some *a priori* information.

Bistatic optical arrangement of sounding allows one, using the anomalous backscattering effect, to isolate the fraction of crystal aerosol that represents oriented plates from a polydisperse ensemble of various composition. Besides, using the capabilities of a scanning lidar, one can obtain high-amplitude specularly reflected signal and to record the change of the polarization state of incident radiation, that bears information about optical, microphysical, and orientation properties of the atmospheric formation under study.

Conclusion

A round water ice plate was considered in order to theoretically study the light scattering characteristics in application to bistatic laser polarization sounding. The principal peculiarities of scattering are presented in this paper, which allow one to select most informative areas in the research of light scattering for interpreting the data of polarization sounding. It was ascertained, based on numerical investigation, that there is a well pronounced dependence of the scattering cross section on the plate radius. Besides, the regular dependence of polarization characteristics on the refractive index of the particulate matter, its orientation, and orientation of the polarization plane has been revealed.

We have shown that in the case of specular reflection from crystals, the procedure of interpreting

the data of bistatic sounding can be simplified essentially because there is no dependence of scattering on some angular characteristics. It is obvious, that to reduce the experiment to the necessary pattern one need to know the peculiarities of scattering different from the specular reflection, in particular, for different positions of source, receiver, and scattering particle.

The following possible approaches to studying physical properties of cirrus clouds have been mentioned in this paper. Using a bistatic polarization lidar together with the proposed numerical model, one can obtain the real-time data on microphysical, optical, and dynamic properties of crystal aerosol. In this case plates are meant as the indicators. Determining their geometrical parameters and orientation, one can assess the structure of a cloud as a whole, because certain plate size, number density, and orientation are related to the specific spectra of shapes and size of other types of crystals. In their turn, these data can be used for prediction of the conditions of propagation of radiation both in geophysics (transfer of solar radiation in the atmosphere) and in applied problems (operation of optical communication and location systems through crystal clouds).

Acknowledgments

The author would like to thank Prof. I.V. Samokhvalov and Prof. A.A. Popov for the support of this work, valuable remarks and advises which favored the improvement of this paper.

The work was supported in part by Russian Foundation for Basic Research (Grant No. 98-02-3031).

References

1. G. Manago and C.W. Lee, J. Fac. Sci. Hokkaido Univ., Ser. 7 (Geophys.), No 2, 321-335 (1966).
2. O.A. Volkovitskii, L.N. Pavlova, and A.G. Petrushin, *Optical Properties of Crystal Clouds* (Gidrometeoizdat, Leningrad, 1984), 200 pp.
3. A. Heymsfield, J. Atm. Sci. **34**, 367-381 (1977).
4. W.A. Cooper and G. Vali, J. Atm. Sci. **38**, 1244-1259 (1981).
5. H.-R. Cho, J.V. Iribarne, and W.G. Richards, J. Atm. Sci. **38**, 1111-1114 (1981).
6. M.V. Kabanov, ed., *Regional Monitoring of the Atmosphere. Part 1. Scientific-Technical Principles* (SB RAS Publishing House, Tomsk, 1997), 211 pp.
7. B.A. Tinsley and G.W. Deen, J. Geophys. Res. **96**, No. D12, 22283-22295 (1991).
8. T.C. Marshall, W.D. Rust, W.P. Winn, and K.E. Gilbert, J. Geophys. Res. **94**, No. D2, 2171-2181 (1989).
9. M.V. Kabanov, ed., *Regional Monitoring of the Atmosphere. Part 2. New Devices and Techniques of Measurement* (SB RAS Publishing House, Tomsk, 1997), 295 pp.
10. V.S. Shamanov and A.I. Abramochkin, "Svetozar-3" airborne polarization laser radar. Construction and application", Preprint No. 15, (Tomsk, 1984), 47 pp.
11. K. Sassen and K.-N. Liou, J. Atm. Sci. **36**, 852-861 (1979).
12. B.M. Welsh and C.S. Gardner, Appl. Opt. **28**, 32-82 (1989).
13. A. Mallmann, J.L. Hock, and R.G. Greenler, Appl. Opt. **37**, 1441-1449 (1998).
14. G.P. Konnen and J. Tinbergen, Appl. Opt. **37**, 1457-1464 (1998).
15. C.M.R. Platt, J.C. Scott, and A.C. Dilley, J. Atm. Sci. **44**, 729-747 (1987).
16. A.A. Popov and O.V. Shefer, Appl. Opt. **33**, 7038-7044 (1994).
17. O.V. Shefer, Atmos. Oceanic Opt. **12**, No. 7, 549-553 (1999).
18. A.A. Popov and O.V. Shefer, Appl. Opt. **34**, 1488-1492 (1995).
19. K.-N. Liou and H. Lahore, J. Appl. Meteorol. **13**, No. 2, 257-263 (1974).
20. A.A. Popov and O.V. Shefer, "On the laser polarization sounding of crystal clouds: the simplest optical models of PARTICLE", Preprint No. 65 (Tomsk, 1988), 59 pp.